Supramolecular Materials 3 (2024) 100062

Contents lists available at ScienceDirect

Supramolecular Materials

journal homepage: www.keaipublishing.com/en/journals/supramolecular-materials/

Fabrication of the polyetherketoneketone-reinforced nano-hydroxyapatite composites as inspired by the cortical bone

Zhongyi Wang [a,b,c,d], Yadong Zhang [e], Junyi Zhao [a], Chenyang Xie [a], Qiang Wei [f,*], Haiyang Yu [a,*]

[a] State Key Laboratory of Oral Diseases, National Clinical Research Center for Oral Diseases, West China Hospital of Stomatology, Sichuan University, Chengdu, Sichuan 610041, China
[b] Department of Periodontics, the Affiliated Stomatological Hospital of Nanjing Medical University, Nanjing, China
[c] Jiangsu Province Key Laboratory of Oral Diseases, Nanjing Medical University, Nanjing, China
[d] Jiangsu Province Engineering Research Center of Stomatological Translational Medicine, Nanjing, China
[e] Zhejiang PEKK-X Advanced Materials Technology Co., Ltd, Shaoxing, Zhejiang 312000, China
[f] College of Polymer Science and Engineering State Key Laboratory of Polymer Materials and Engineering Sichuan University Chengdu, Sichuan 610065, China

ARTICLE INFO

Keywords:
Polyetherketoneketone
Nano-hydroxyapatite
Cortical bone
Bioinspired composites
Freeze-casting

ABSTRACT

Cortical bone has superior mechanical performance. Hydroxyapatite (HA) as its main component are attractive bioactive materials, but possess weak strength. The critical factor is the difference in the structure. Inspired by the hierarchical and delicate architecture of the cortical bone, we used a slurry with 2 wt% polyvinyl alcohol (PVA) and 20 vol% polydopamine-modified nano HA (nHA, pDA-nHA) to fabricate stronger scaffolds characterized by a lamellar structure. Additionally, we immersed the pDA-nHA scaffolds into the polyetherketoneketone (PEKK) synthesis system to reinforce the scaffolds. The cortical bone-inspired composites were produced successfully, and the 20 vol% pDA-nHA+2 wt% PVA/PEKK composites had the highest strength and modulus. It provides a new solution for enhancing the mechanical strength of the single component, as well as improving the bioactivity of PEKK.

1. Introduction

Cortical bone develops a part of the bone with the highest stiffness and toughness and is fundamental to protection, locomotion, storage depot, etc. [6]. These features can be attributed to at least three advantages of structures: (1) it is mainly composed of 65 wt% mineral and 25 wt% organics, arranged hierarchically; (2) nano hydroxyapatite (nHA) crystals nucleate regularly and in a directed manner; (3) it can be distinguished into five structures from nano- to macro-structures [16,17]. The mineral phase provides stiffness and hardness that is combined with a minor organic phase to acquire softness and toughness. The elaborate architecture compensates for the weakness of ceramic components and is an important method for designing hybrid materials. With the $Ca_{10}(PO4)_6(OH)_2$ chemical formula, HA is the main inorganic component of the bone. Up to now, a single component of nHA materials has shown weak mechanical properties [9]. Studies using the mixing method to reinforce HA could hardly acquire high strength and content simultaneously, which is important for improving the bioactivity of composites [1,12,13]. These problems have limited the applications of HA in tissue engineering.

Freeze-casting technology can produce complex hierarchical materials by ice template, which is environmentally friendly [15]. It has been proven effective in creating high-performance HA/poly(methyl methacrylate) (PMMA) composites with hierarchical "brick-and-mortar" architectures [4]. Polyetherketoneketone (PEKK) is a member of the Food and Drug Administration (FDA)-approved high-performance

Abbreviations: Hydroxyapatite, (HA); polyvinyl alcohol, (PVA); polydopamine-modified nano HA, (nHA, pDA-nHA); Dopamine, (DA); polyetherketoneketone, (PEKK); poly(methyl methacrylate), (PMMA); polyaryletherketone, (PAEK); isophthaloyl dichloride, (IPC); terephthaloyl chloride, (TPC); 1-Methyl-2-pyrrolidinone, (NMP); diphenyl ether, (DPE); energy-dispersive X-ray spectroscopy, (EDS); transmission electron microscopy, (TEM); X-ray diffraction, (XRD); Thermogravimetric analysis, (TGA); differential scanning calorimetry, (DSC); Fourier-transform infrared spectroscopy, (FTIR); focused ion beam, (FIB); high-angle annular dark-field, (HAADF); three-dimensional, (3D); scanning probe microscopy, (SPM); mHA, (micro-HA).

* Corresponding authors.
E-mail addresses: wei@scu.edu.cn (Q. Wei), yhyang6812@scu.edu.cn (H. Yu).

https://doi.org/10.1016/j.supmat.2023.100062
Received 26 November 2023; Received in revised form 12 December 2023; Accepted 21 December 2023
Available online 14 January 2024

polyaryletherketone (PAEK) polymer family, which is at the forefront of dentistry and biomaterial science [10,14]. It contains ether and ketone groups and has chemical stability in our internal environment [10]. It also exhibits an elastic modulus similar to bone and high mechanical strength [2]. Thus, PEKK is an ideal organic component to reinforce the nHA scaffolds.

Nanomaterials are well proven to have enhanced mechanical properties, on account of the large specific surface area and quantum effect [21]. However, nanoparticles tend to agglomerate by strong van der Waals attraction, which are dispersed inhomogeneously in aqueous slurries. Dopamine (DA) is a mussel-inspired catecholamine, which can self-polymerize to form a poly-(DA) (pDA) film to adhere to particles. Studies have found that pDA-modified particles can disperse well [7,18]. Thus, pDA-modified nHA (pDA-nHA) is used to build scaffolds. Considering the limited mechanical strength and osteoinductive ability of pure pDA-HA or sintered pDA-nHA bioactive ceramics, synthesizing composite materials is a mainstream solution [11,19].

Thus, we fabricated nHA scaffolds using freeze-casting technology and innovatively produced nHA/PEKK composites by in situ polymerization of PEKK. The nHA scaffolds provided good osteoinductive ability, while the limited mechanical strength could be made up by PEKK. Then, mechanical and surface characterizations were further explored. This study is believed to provide more application potential for bone tissue engineering of nHA.

2. Material and methods

2.1. Synthesis of pDA-nHA

20 mg/mL nHA (density = 2.3 g/cm^3 and particle size ≈ 20 × 100 nm, Nanjing Emperor Nano Material Co., Ltd., China) and DA hydrochloride (Beijing Solabao Technology Co., Ltd., China) were ultrasonically dispersed in Tris buffer (10 mM, pH 8.5). The core-shell particles were obtained from 4, 6, 8, 10, and 12 mg/mL DA solutions as 4pDA-nHA, 6pDA-nHA, 8pDA-nHA, 10 pDA-nHA, and 12 pDA-nHA, respectively, to investigate the optimum shell thickness of PDA-coated HANPs. After stirring at room temperature for 12 h, the modified nHA was purified by centrifugation, then dried and ground for use.

2.2. Fabrication of environmently friendly Lamellar nHA Scaffolds

The lamellar structure was formed via the environmentally friendly ice-templated technique, realized by a homebrew directional freezing machine with a controllable cooling rate. Slurries with ceramic-to-water volume ratios of 10, 15, and 20% were prepared by mixing nHA (density = 2.3 g/cm^3 and particle size ≈ 20 × 100 nm, Nanjing Emperor Nano Material Co., Ltd., China) or pDA-nHA in deionized water with the addition of 0.5 wt% hydroxyethyl cellulose (H300, Lotte Co., Ltd, Korea), 0.75 wt% Dynol 604 (Air Products & Chemicals Inc., USA), and 1.5 or 2 wt% PVA 1788 (Chengdu Kelong Chemical Co., Ltd, China). The slurries were ultrasonically blended and then poured into a teflon mold, the bottom of which was the copper cold finger. The top of the cold finger had a heat detector with a ring heater and was immersed in liquid nitrogen. The heat detector changed the temperature of the mold copper base according to the preset cooling rate (2.5 °C/min) feedback to heat the ring. The frozen samples were freeze-dried in a vacuum freeze dryer (SP SCIENTIFIC, Warminster, PA, USA) for 1 week, pre-fired at 500 °C for 2 h in a Sintering Furnace (AGT/S, Aidite,Qinhuangdao, China) to remove the organics, and then, sintered at 1350 °C for 3 h to form the lamellar structures.

2.3. Preparation of nHA/PEKK and pDA-nHA/PEKK composites

The nHA/pDA-nHA scaffolds were modified with γ-MPS by immersing them into the 1 wt% γ-MPS/ethanol solution for 24 h. After grafting with γ-MPS, scaffolds were dried at 40 °C for 24 h. Then, nHA/PEKK and pDA-nHA/PEKK composites were synthesized via in situ polymerization of PEKK under a nitrogen atmosphere. In the next step, the composites were heat-treated at 380 °C for 30 min under an argon atmosphere to melt the PEKK particles to form a combination with the scaffolds.

2.4. In situ polymerization of PEKK

Scaffolds, 0.04 mol isophthaloyl dichloride (IPC), 0.14 mol terephthaloyl chloride (TPC), 0.5 mol 1-Methyl-2-pyrrolidinone (NMP), 0.2 mol diphenyl ether (DPE), and 600 mL dichloroethane were poured into a 2 L reactor equipped with an N_2 inlet and stirred until the temperature dropped to −15 °C. Then, 104 g (0.78 mol) $AlCl_3$ was slowly poured into the reaction mixture, and the reactor contents were stirred for 2 h at −15 °C. Next, the temperature was raised to 22 °C and stirred for 24 h. The composites were then taken out and immersed in methanol for 2 h. Afterward, the composites were refluxed twice in methanol for 4 h and deionized water for 24 h, and dried at 150 °C for 6 h.

2.5. Material characterization

The microstructure of the scaffolds and composites was characterized using environmental scanning electron microscopy (ESEM, JSM-IT500, JEOL, Japan) after a gold coating was added to the surface of the samples. The surface constituents were characterized using energy-dispersive X-ray spectroscopy (EDS, JSM-IT500, JEOL, Japan). The pore width and lamella thickness of the scaffolds were measured using the Nano Measure 1.2 software (Fudan University, Shanghai, China) based on SEM images. The morphology and distribution of nanopowders were characterized by transmission electron microscopy (TEM, JEM-2100Plus, Japan). The zeta potential and size of these particles in the aqueous solution were analyzed using a Zetasizer 3000HS (Malvern Instruments Ltd, Malvern, UK) and an LS230 laser diffraction particle size analyzer (Beckman Coulter Inc., Brea, CA, USA), respectively. X-ray diffraction (XRD) analyses were conducted using an X-ray diffractometer (D8 Advance, Bruker AXS, Germany) in the 10–80° diffraction range and a scanning rate of 5° min^{-1}. Thermogravimetric analysis (TGA) and differential scanning calorimetry (DSC) were conducted using a Thermogravimetric analyzer (Perkin-Elmer 7, USA) under a nitrogen atmosphere with a heating rate of 10 °C min-1. Fourier-transform infrared spectroscopy (FTIR) was performed using an infrared spectrometer (Boguang Technology Co. Ltd., Shanghai, China). The cortical bone slices were cut via a focused ion beam (FIB, FEI Strata 400S, USA), and a high-angle annular dark-field (HAADF) scanning transmission electron microscopy mode (STEM) image of the sliced specimens was obtained using TEM.

2.6. Mechanical properties

Compression tests were performed using an Instron testing machine (Instron 3400; Instron, MA, US) at room temperature. Cylindrical samples were prepared for monotonic compression tests with a displacement rate of 0.5 mm min^{-1}.

Three-dimensional (3D) topography of the surface of materials was observed using a white light interferometer 3D surface profilometer (RTEC, USA). Moreover, the surface roughness was measured by Gwyddion 2.30 open-source software, developed for analyzing scanning probe microscopy (SPM, Czech Metrology Institute, Brno, Czech Republic).

Young's modulus and hardness were measured using an indentation test via the TriboIndenter system (Hysitron Inc. TI950, Minneapolis, MN, USA) with a load of 6000 μN and a trapezoid function, including a linear loading period, a hold period at the peak load, and an unloading period for 20 s each on polished samples up to 1 μm.

2.7. Statistical analysis

Numerical data are presented as the mean and standard deviation (mean ± SD). The SPSS 24.0 software (SPSS Inc., Chicago, USA) was used to analyze the differences among the groups using a one-way ANOVA. A P value < 0.05 was considered statistically significant. Statistical analysis was performed using GraphPad Prism 5.01 (GraphPad Software, La Jolla, CA).

3. Results

3.1. Preparation of pDA-nHA particles

nHA was immersed in different concentrations of pDA solutions to select the optimal dispersibility of pDA-nHA. As shown in Fig. 1A, rod-like nHA coated by pDA could decrease the agglomeration trend. 8pDA-nHA in the 8 g/L pDA solution had the smallest hydrodynamic of 325 nm, while nHA had the largest hydrodynamic diameter of 1819 nm (Table 1). nHA with different contents of the pDA coating was observed in an aqueous solution at different time intervals to investigate the suspension stabilities of particles. The color of the 8pDA-nHA was the brownest, and nHA descended to the bottom slowly. This indicates that the pDA coating could reduce the sedimentation rate and maintain a stable dispersion, especially 8pDA-nHA (Fig. 1B). The FTIR spectra of particles were analyzed. All the particles had the peaks at wavenumbers of ~565, ~603, ~1035, and ~1091 cm^{-1}, which are ascribed to the

Table 1
Average hydrodynamic size and zeta potential of particles ($n = 3$).

	nHA	4pDA-nHA	6pDA-nHA	8pDA-nHA	10pDA-nHA	12pDA-nHA
Average hydrodynamic diameter (nm)	1819	622	613	325	658.3	737.4
Average zeta-potential (mV)	−8	−16	−14	−16.1	−15.9	−14.5

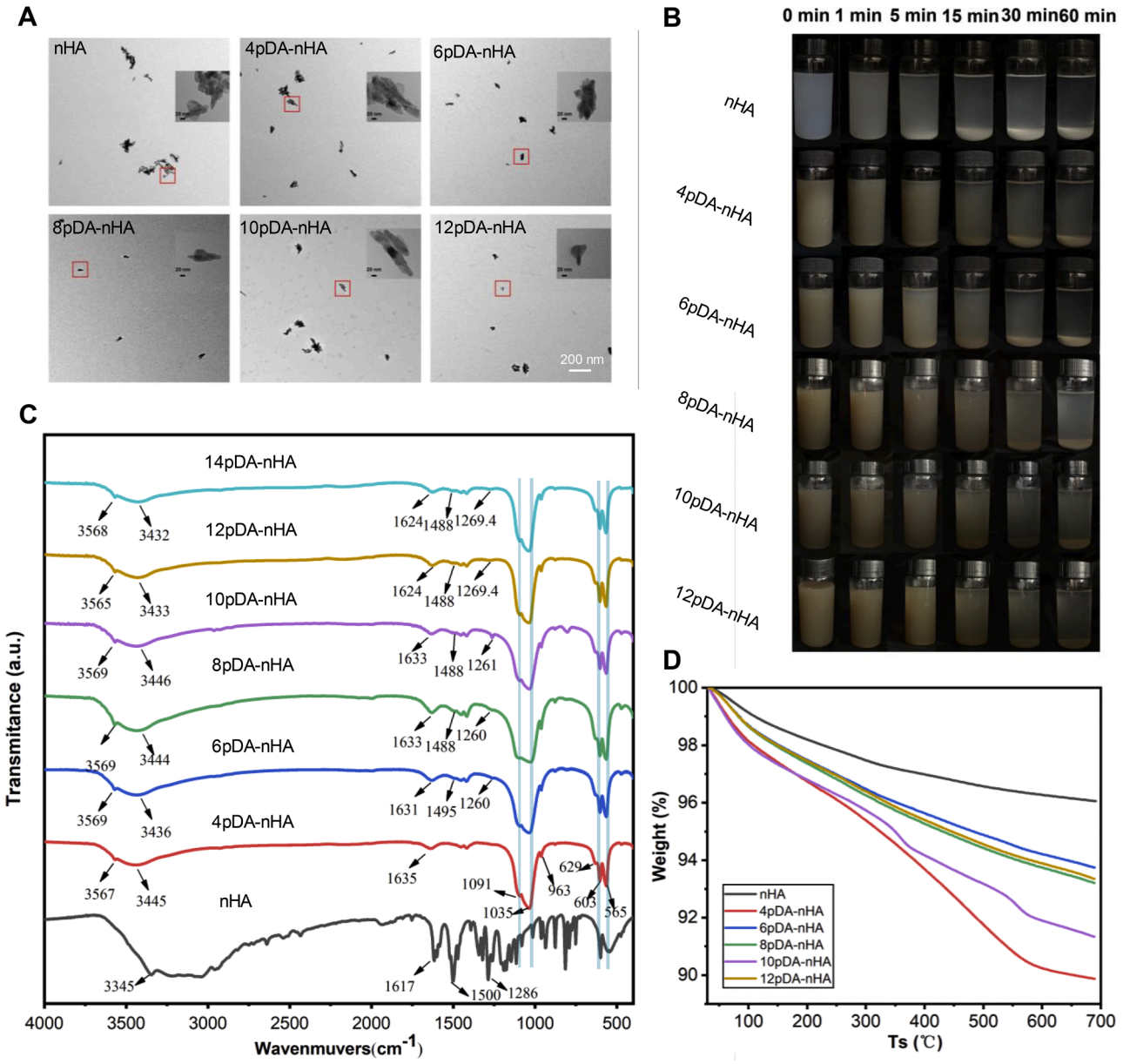

Fig. 1. Characterization of nHA and particles modified with 0, 4, 6, 8, 10, and 12 g/L pDA solution. (A) TEM images. (B) Particle dispersibility in ultrapure water. (C) FTIR spectra of particles. (D) TGA curves of particles.

presence of PO_4^{3-} group, as a standard profile of HA [22].The peaks at ~1488 and ~1633 cm^{-1} correspond to the N—H bending and shearing vibration and the overlap of C = C resonance vibration in pDA [18] (Fig. 1C). According to the thermogravimetric (TGA) measurements, the grafting ratio of the 4, 6, 8, 10, 12pDA-nHA were 6.18%, 2.31%, 2.86%, 4.72%, 2.7% respectively (Fig. 1D). These phenomena verified the success of pDA modification.

3.2. Fabrication of nHA/PEKK composites

The dark-field images of the ion-milled sections of cortical bone show the oriented nHA crystals characterized by scattered electrons from a specific lattice plane. Collagen fibrils were closely filled among the hierarchical structures of minerals (Fig. 2A, B). Inspired by the decent arrangement of cortical bone, we fabricated the hierarchical architecture of the pDA-nHA scaffolds by the vertical temperature gradient (ΔT), which could force the growth of the ice nucleus. The sintered scaffolds were immersed into the synthesis system of PEKK. Considering that the melting point of PEKK was above 355 °C, the composites were heated to 380 °C to enhance PEKK filling between lamella ceramics (Fig. 2C, D). Moreover, we also produced nHA/PEKK composites to investigate the role of microstructure related to the pDA coating. The SEM images proved that the PEKK connectively bonded to nHA/pDA-nHA scaffolds (Fig. 2E). The EDS images of 10%pDA-nHA+2% PVA/PEKK present the PEKK distribution in the composites (Fig. 2F). The FTIR spectra of PEKK shows the formation of C = O at 1645 cm^{-1}, the C—O-C stretching vibration of diaryl bands at 1199 and 1236 cm^{-1}, and the diphenyl ketone bands at 1491 and 1588 cm^{-1} (Fig. 2G) [26]. Moreover, we analyzed the patterns of particles, scaffolds, and PEKK. The characteristic peaks of $Ca_{10}(PO4)_6(OH)_2$ (PDF#09–0432) occurred on particles and scaffolds. The PEKK had a typical peak, as presented by PDF#52–2277 (Fig. 2H).

3.3. Selection by SEM and compression test

To preliminary identify the cross-sectional microstructure and mechanical property of nHA and pva component, we explored nHA+1.5% pva, nHA+2% pva and micro-HA(m-HA)+1.5% pva by compression test (Fig. S1). nHA scaffolds have more uniform thickness lamellae, and therefore were significantly superior to micro-HA scaffolds in compressive strength. Pva component is also of importance in increase the strength by enhanced thickness of lamellae and lamellar lateral branches. To comprehensively explored the objective law of microstructure and strength of nHA scaffolds with 1.5% or 2% pva, and with or without pDA modified, we observed the cross-sectional microstructure (Fig. 3A and Table 2) and compressive strength and modulus (Figs. 3B-E) of nHA and pDA-nHA scaffolds and corresponding composites with different mineral and PVA contents. Moreover, the typical stress-strain curves of scaffolds and composites are presented in Fig. 3F and 3G respectively. pDA-nHA scaffolds obviously had thinner lamella thickness and pore width than nHA scaffolds but had more lamellae and were compact. The 2 wt% PVA content in the slurry could improve the thickness of lamellae and, therefore, enhance the scaffolds and the corresponding composites. Based on the 2 wt% PVA content, the 20 vol % pDA-nHA scaffolds presented the highest compressive strength of 12.72 ± 1.37 MPa and compressive modulus of 801.07 ± 63.53 MPa. Moreover, the in situ polymerization of PEKK supported the mineral component and acquired a brick-and-mortar composite. The stable structure could assist in achieving much more compressive strength and modulus compared to a single component. The compressive strength of 20%pDA-nHA+2% PVA/PEKK was the highest, 22.84 ± 2.67 MPa, and its modulus was also the highest, 905.27 ± 34.52 MPa. The stress-strain behavior were linear elastic until failure due to lamellar fracture and/or HA/PEKK delamination under the loading nose. The strain of composites at failure are higher than corresponding scaffolds, indicating the significance of PEKK component.

3.4. The surface characteristics of 20%pDA-nHA+2%PVA/PEKK

20%pDA-nHA+2%PVA/PEKK was found to be the strongest among tested materials. Thus, we explored its surface characteristics and compared them with 20%nHA+2%PVA/PEKK. The 3D topography of the surface is shown in Fig. 4A. The surface roughness of 20%pDA-nHA+2%PVA/PEKK was 40.95 ± 11.92 nm, lower than 20%nHA+2% PVA/PEKK (60.98 ± 12.61 nm) (Fig. 4B). 20%pDA-nHA+2%PVA/PEKK had lower water contact angle (64.03 ± 1.77°) than 20%nHA+2%PVA/PEKK (70.84 ± 3.76°), indicating its better hydrophilicity (Fig. 4C). The 20%pDA-nHA+2%PVA/PEKK had Young's modulus (14.13 ± 3.49 GPa) and hardness (365.95 ± 151.42 MPa) comparable to the cortical bone, and higher than PEKK (Fig. 4D). As shown in the ashby plot (Fig. 4E), melt blending build the lowest strength. The HA particles synthesized toghther with PEKK (synthesized HA/PEKK Hybrids) and 20%pDA-nHA+2%PVA/PEKK have comparable strength to cortical bone ([5,12,13]; X. [23]). For the composites in our work were fabricated by in situ polymerization, the hardness and Young's modulus are in a wide range.

4. Discussion

Freeze-casting technology is environmentally friendly for using water adequately to build ice templates, which will later be replaced by aligned 3D porous networks. The technology has been well applied to construct hierarchically biomimetic materials inspired by nature ([15]; Zhao et al., 2022). It is an easy and available technology for various materials, such as metals, ceramics, and polymers ([8]; H.-P. [24,25]). The micro- to macro-size of materials can also be easily adjusted according to the requirements. The multiple-length scales can be achieved by modifying ice crystal morphology with cooling rate, additives, or/and freezing finger conditions [3]. nHA scaffolds were used in this research for their compressive strength were superior to mHA (micro-HA) (Fig. S1). According to our previous study, pDA coating can decrease slurry viscosity and the agglomeration tendency [20]. As shown in Fig. 1, pDA-nHA slurry dispersed well and was easier to acquire homogeneous dispersion in the aqueous slurry, compared with nHA (Fig. 1 and Table 1). According to average hydrodynamic size and the grafting ratio of nHA modified with different concentrations of pDA solution, both tendency is from high to low to high. This may because the too high concentration may influence the coating of pDA. Moreover, too high grafting ratio is not benefit for a stable dispersion. Accordingly, 8pDA-nHA is favorable. Thus, 8pDA-nHA slurry is more easier to achieve a lower resistance to ice nucleation and a faster vertical nucleation rate, generating more ice nuclei quickly in this article [3]. In a limited space, they resulted in the formation of more ice lamellae, later substituted by pores and thinner lamellae of ceramics. As shown in Fig. 2E, 3A and Table 2, both pva and HA content can contribute to high lamella thickness and more lamellar lateral branches, indicating the increased slurry viscosity and accompanied resistance of ice nucleation. Slurry with a 2% PVA content could build thicker and stronger scaffolds than 1.5%. Meanwhile, the pDA-nHA can optimize the spatial structure and achieve the ability to resist destruction. Thus, the pDA-nHA and 2 wt % PVA are preferred in this research.

Inspired by the complex architecture of the cortical bone, PEKK was introduced to reinforce the mechanical strength of nHA and pDA scaffolds (Fig. 2A, B). PEKK has excellent fracture resistance, shock absorption, and stress distribution and is a potential alternative to metals in clinical applications [14]. However, its application in bioactive materials is limited to its bio-inertia. Hence, our nHA/PEKK and pDA-nHA/PEKK composites emerged to fulfill better biological functions (Fig. 2C, D). Combining the SEM and EDS images, the PEKK was filled well between ceramics and closely connected (Fig. 2E, F). The FTIR spectra and XRD patterns verified the successful synthesis of the composites. The sintered pDA-nHA scaffolds were still the $Ca_{10}(PO4)_6(OH)_2$ (PDF#09–0432) (Fig. 2G, H).

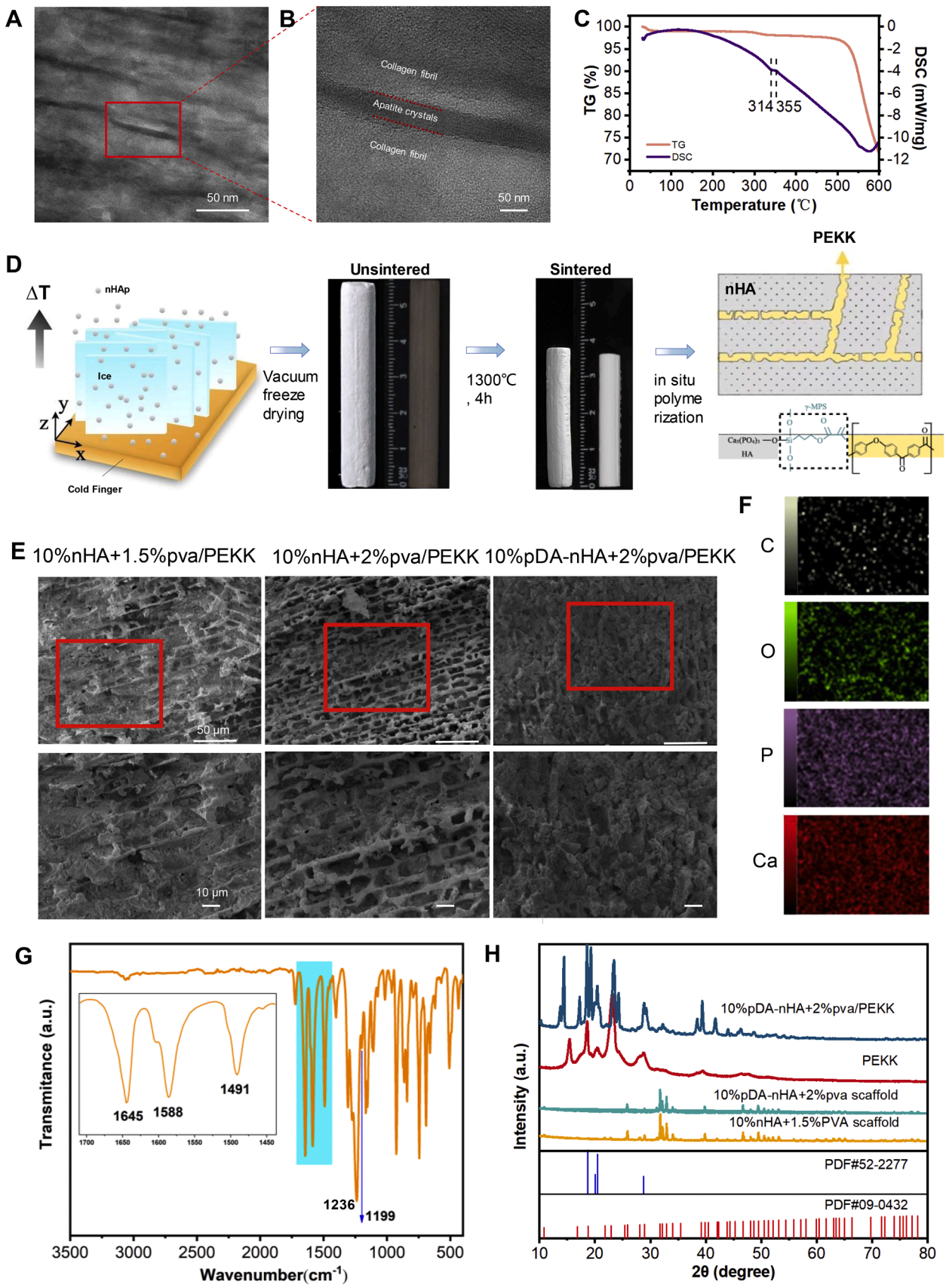

Fig. 2. The cortical bone and synthesis of cortical bone-inspired composites. (A) TEM images of the cortical bone in an edentulous area. (B) The enlarged TEM image taken from the red zone in (A). (C) Combined TGA/DSC curves of PEKK. (D) The schematic illustration of the synthesis process of nHA/PEKK composites. (E) The cross-sectional scanning of SEM images of nHA/PEKK composites (×500, and enlarged ×1000). (F) EDS of 10%pDA-nHA+2%PVA/PEKK. (G) FTIR spectra of PEKK. (H) XRD patterns of 10%pDA-nHA+2%PVA/PEKK, PEKK, 10%pDA-nHA+2%PVA scaffold, and 10%nHA+1.5%PVA scaffold.

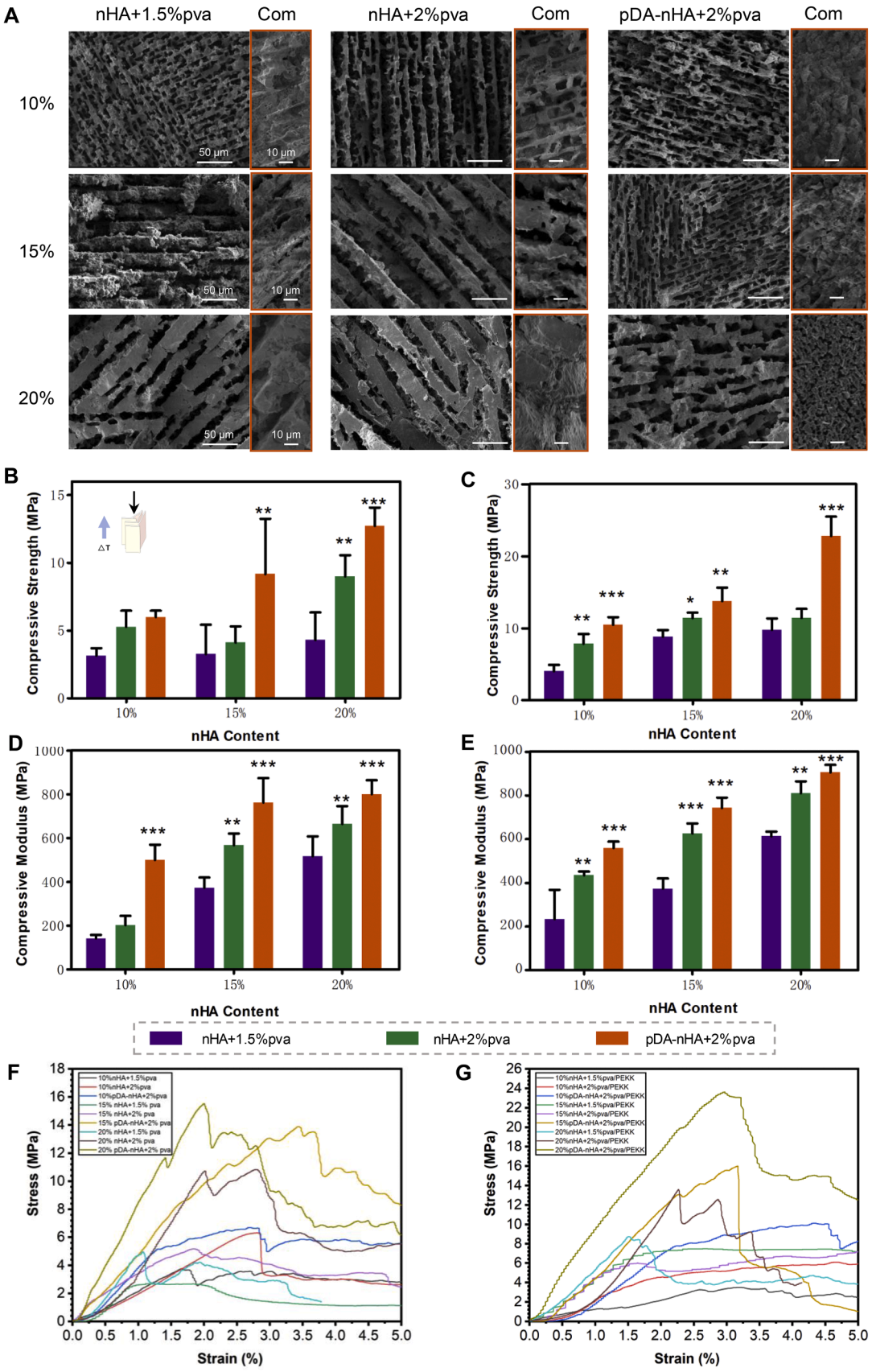

Fig. 3. SEM images and the compression test of nHA scaffolds and nHA/PEKK composites. (A) Cross-sectional SEM images (×500); Composites (Com) are shown in the orange box (×1000). The compressive strength and modulus of (B, D) the lamellar nHA scaffolds and (C, E) nHA/PEKK composites parallel to the freezing direction. The typical stress-strain curves of (F) scaffolds and (G) composites in the compression test.

Table 2
The pore width and lamella thickness of the lamellar nHA and pDA- nHA scaffolds with different particle and PVA contents perpendicular to the freezing direction (mean ± SD, $n = 14$).

	Pore width (μm)	Lamella thickness (μm)
10% nHA+1.5% pva	8.67 ± 2.11	2.06 ± 1.05
10% nHA+2% pva	8.82±0.97	4.60 ± 1.07
10% pDA-nHA+2% pva	9.62±1.40	2.24±1.10
15% n-HA+1.5% pva	12.09 ± 2.22	18.86 ± 2.58
15% n-HA+2% pva	14.52 ± 1.78	19.39 ± 2.24
15% pDA-nHA+2% pva	9.60 ± 2.48	3.70 ± 1.41
20% nHA+1.5% pva	12.63 ± 1.84	16.84 ± 4.04
20% nHA+2% pva	13.67 ± 3.02	16.93 ± 3.96
20% pDA-nHA+2% pva	12.48 ± 2.26	10.28 ± 3.18

As shown in Fig. 3B-G, the compressive strength and modulus of scaffolds and composites had the same tendency. Adding 2 wt% PVA and the pDA coating could increase the strength of materials. The 20% pDA-nHA+2%PVA/PEKK composites had the highest compressive strength, 22.84 ± 2.67 MPa, and the 10% nHA+1.5%PVA/PEKK had the lowest, 4.03 ± 0.87 MPa. As shown in Fig. 4A-D, the mechanical test of the interface showed that 20%pDA-nHA+2%PVA/PEKK could achieve a smoother and more hydrophilic surface, as well as higher Young's modulus and hardness. In Fig. 4E, 20% pDA-nHA+2%PVA/PEKK have large value range of hardness and Young's modulus, indicating its heteropical structure. This is because the composites are composed by nHA scaffolds and PEKK in situ polymerization at the micro scale, while nanoindentation tests are operated at nano scale. The experimental data is credible. We also can see that the strength of composites in our work

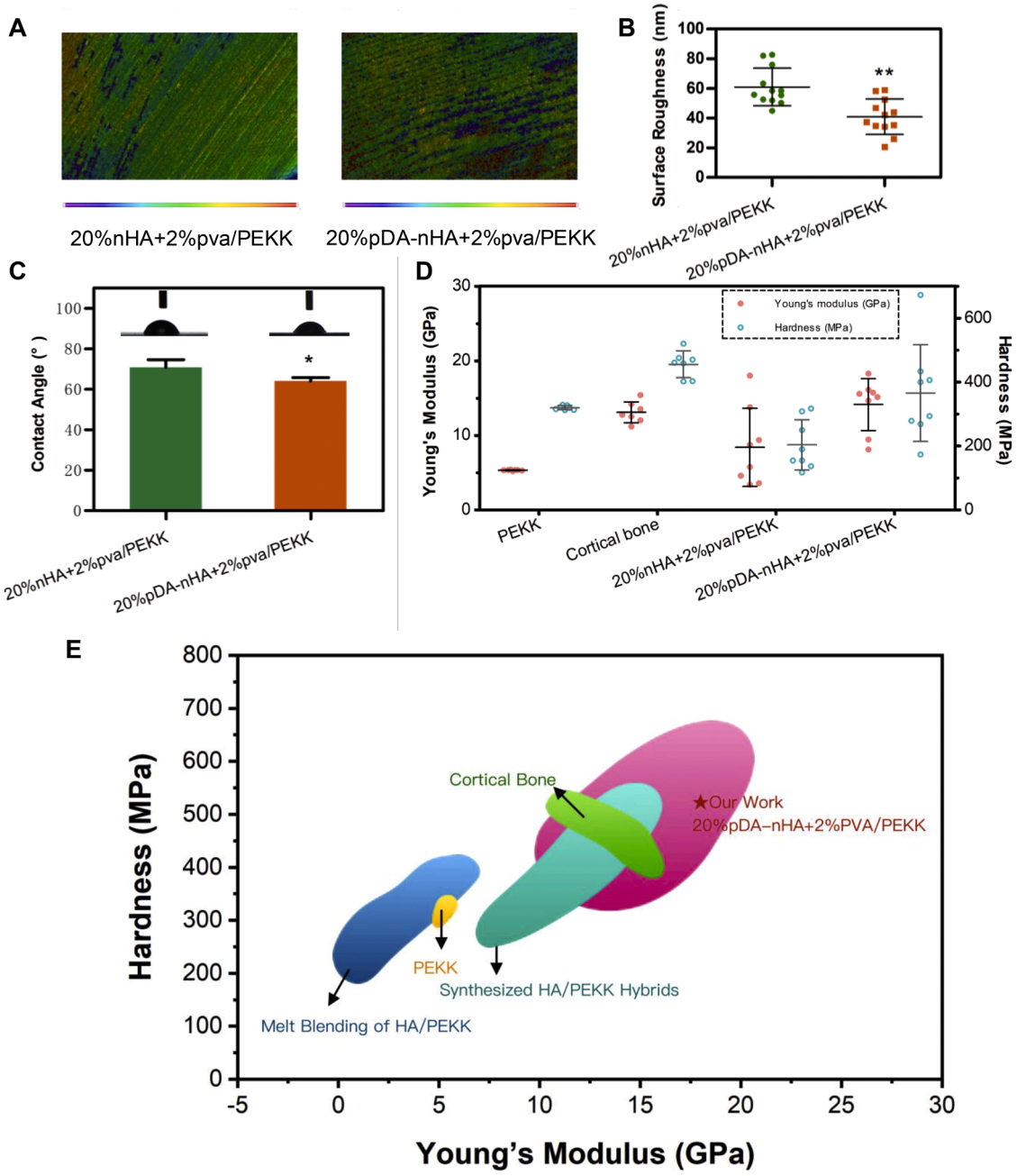

Fig. 4. The surface characteristics of 20%pDA-nHA+2%PVA/PEKK. (A) The 3D topography of the surface, and (B) the surface roughness of materials. (C) The water contact angle of materials. (D) Young's modulus and hardness were measured by the nanoindentation test. (E) The ashby plot of 20%pDA-nHA+2%PVA/PEKK and related materials.

are comparable, even higher, to cortical bone. Thus, these novel biomimetic engineering materials are supposed to help the single component for more clinical applications.

5. Conclusion

In summary, the PVA content and the homogeneous dispersion of the slurry are important for the microstructure of the freeze-casting scaffolds. The novel 20% pDA-nHA+2%PVA/PEKK composites were developed with a biomimetic architecture and high strength and modulus. It is a promising prospect for clinical applications.

Declaration of competing interest

The authors declare that they have no known competing financial interests or personal relationships that could have appeared to influence the work reported in this paper.

Acknowledgments

This work was financially supported by the National Natural Science Foundation of China (No. 82071145) and the Research Fund of Interdisciplinary Innovation Project fromWest China Hospital of Stomatology, Sichuan University (RD-03-202009).

Supplementary materials

Supplementary material associated with this article can be found, in the online version, at doi:10.1016/j.supmat.2023.100062.

References

[1] H. Ait Said, H. Mabroum, M. Lahcini, H. Oudadesse, A. Barroug, H. Ben Youcef, H Noukrati, Manufacturing methods, properties, and potential applications in bone tissue regeneration of hydroxyapatite-chitosan biocomposites: a review, Int. J. Biol. Macromol. 243 (2023) 125150, https://doi.org/10.1016/j.ijbiomac.2023.125150.
[2] H. Alqurashi, Z. Khurshid, A.U.Y. Syed, S. Rashid Habib, D. Rokaya, M.S. Zafar, Polyetherketoneketone (PEKK): an emerging biomaterial for oral implants and dental prostheses, J. Adv. Res. 28 (2021) 87–95, https://doi.org/10.1016/j.jare.2020.09.004.
[3] H. Bai, Y. Chen, B. Delattre, A.P. Tomsia, R.O. Ritchie, Bioinspired large-scale aligned porous materials assembled with dual temperature gradients, Sci. Adv. 1 (11) (2015) e1500849, https://doi.org/10.1126/sciadv.1500849.
[4] H. Bai, F. Walsh, B. Gludovatz, B. Delattre, C. Huang, Y. Chen, A.P. Tomsia, R. O. Ritchie, Bioinspired hydroxyapatite/poly(methyl methacrylate) composite with a nacre-mimetic architecture by a bidirectional freezing method, Adv. Mater. 28 (1) (2016) 50–56, https://doi.org/10.1002/adma.201504313.
[5] F.E. Baştan, Fabrication and characterization of an electrostatically bonded PEEK-hydroxyapatite composites for biomedical applications, J. Biomed. Mater. Res. B Appl. Biomater. 108 (6) (2020) 2513–2527, https://doi.org/10.1002/jbm.b.34583.
[6] A. Bharadwaz, A.C. Jayasuriya, Recent trends in the application of widely used natural and synthetic polymer nanocomposites in bone tissue regeneration, Mater. Sci. Eng. C. Mater. Biol. Appl. 110 (2020) 110698, https://doi.org/10.1016/j.msec.2020.110698.
[7] F. Cao, P. Jiang, J. Wang, F. Yan, Surface functionalizing effect of fillers on the tribological properties of MWCNT reinforcement HSGFs/phenolic laminate composites under water lubrication, Polym. Adv. Technol. 29 (2) (2018) 767–774, https://doi.org/10.1002/pat.4182.
[8] Z. Chen, X. Liu, T. Shen, C. Wu, L. Zhang, Template-assisted freeze casting of macroporous Ti6Al4V scaffolds with long-range order lamellar structure, Mater. Lett. 264 (2020), https://doi.org/10.1016/j.matlet.2020.127374.
[9] T.M.G. Chu, D.G. Orton, S.J. Hollister, S.E. Feinberg, J.W. Halloran, Mechanical and in vivo performance of hydroxyapatite implants with controlled architectures, Biomaterials 23 (5) (2002) 1283–1293, https://doi.org/10.1016/S0142-9612(01)00243-5.
[10] G.L. Converse, T.L. Conrad, C.H. Merrill, R.K. Roeder, Hydroxyapatite whisker-reinforced polyetherketoneketone bone ingrowth scaffolds, Acta Biomater. 6 (3) (2010) 856–863, https://doi.org/10.1016/j.actbio.2009.08.004.
[11] I. da Silva Brum, L. Frigo, P. Goncalo Pinto Dos Santos, C. Nelson Elias, G. da Fonseca, J. Jose de Carvalho, Performance of nano-hydroxyapatite/beta-tricalcium phosphate and xenogenic hydroxyapatite on bone regeneration in rat calvarial defects: histomorphometric, immunohistochemical and ultrastructural analysis, Int. J. Nanomedicine 16 (2021) 3473–3485, https://doi.org/10.2147/IJN.S301470.
[12] W. Lu, C. Li, J. Wu, Z. Ma, Y. Zhang, T. Xin, X. Liu, S. Chen, Preparation and characterization of a polyetherketoneketone/hydroxyapatite hybrid for dental applications, J. Funct. Biomater. 13 (4) (2022), https://doi.org/10.3390/jfb13040220.
[13] R. Ma, Q. Li, L. Wang, X. Zhang, L. Fang, Z. Luo, B. Xue, L. Ma, Mechanical properties and in vivo study of modified-hydroxyapatite/polyetheretherketone biocomposites, Mater. Sci. Eng. C. Mater. Biol. Appl. 73 (2017) 429–439, https://doi.org/10.1016/j.msec.2016.12.076.
[14] L.M. Maloo, S.H. Toshniwal, A. Reche, P. Paul, M.B. Wanjari, A sneak peek toward polyaryletherketone (PAEK) polymer: a review, Cureus. 14 (11) (2022) e31042, https://doi.org/10.7759/cureus.31042.
[15] E. Munch, M.E. Launey, D.H. Alsem, E. Saiz, A.P. Tomsia, R.O. Ritchie, Tough, bio-inspired hybrid materials, Science (1979) 322 (5907) (2008) 1516–1520, https://doi.org/10.1126/science.1164865.
[16] S. Pang, H.P. Schwarcz, I. Jasiuk, Interfacial bonding between mineral platelets in bone and its effect on mechanical properties of bone, J. Mech. Behav. Biomed. Mater. 113 (2021) 104132, https://doi.org/10.1016/j.jmbbm.2020.104132.
[17] M.A. Rubin, I. Jasiuk, The TEM characterization of the lamellar structure of osteoporotic human trabecular bone, Micron. 36 (7–8) (2005) 653–664, https://doi.org/10.1016/j.micron.2005.07.010.
[18] H. Sun, M. Ai, S. Zhu, X. Jia, Q. Cai, X. Yang, Polylactide–hydroxyapatite nanocomposites with highly improved interfacial adhesion via mussel-inspired polydopamine surface modification, RSC. Adv. 5 (116) (2015) 95631–95642, https://doi.org/10.1039/c5ra21010k.
[19] S. Swain, R. Bhaskar, M.K. Gupta, S. Sharma, S. Dasgupta, A. Kumar, P. Kumar, Mechanical, electrical, and biological properties of mechanochemically processed hydroxyapatite ceramics, Nanomaterials. (Basel) (9) (2021) 11, https://doi.org/10.3390/nano11092216.
[20] Z. Wang, Q. Xiang, X. Tan, Y. Zhang, H. Zhu, J. Pu, J. Sun, M. Sun, Y. Wang, Q. Wei, H. Yu, Functionalized cortical bone-inspired composites adapt to the mechanical and biological properties of the edentulous area to resist fretting wear, Adv. Sci. (Weinh) (2023) e2207255, https://doi.org/10.1002/advs.202207255.
[21] Q. Wu, W.-s. Miao, Y.-d. Zhang, H.-j. Gao, D. Hui, Mechanical properties of nanomaterials: a review, Nanotechnol. Rev. 9 (1) (2020) 259–273, https://doi.org/10.1515/ntrev-2020-0021.
[22] W.F. Yang, L. Long, R. Wang, D. Chen, S. Duan, F.J. Xu, Surface-modified hydroxyapatite nanoparticle-reinforced polylactides for three-dimensional printed bone tissue engineering scaffolds, J. Biomed. Nanotechnol. 14 (2) (2018) 294–303, https://doi.org/10.1166/jbn.2018.2495.
[23] H.-P. Yu, Y.-J. Zhu, Z.-C. Xiong, B.-Q. Lu, Bioinspired fiberboard-and-mortar structural nanocomposite based on ultralong hydroxyapatite nanowires with high mechanical performance, Chem. Eng. J. 399 (2020), https://doi.org/10.1016/j.cej.2020.125666.
[24] X. Yu, S. Yao, C. Chen, J. Wang, Y. Li, Y. Wang, A. Khademhosseini, J. Wan, Q. Wu, Preparation of poly(ether-ether-ketone)/nanohydroxyapatite composites with improved mechanical performance and biointerfacial affinity, ACS. Omega 5 (45) (2020) 29398–29406, https://doi.org/10.1021/acsomega.0c04257.
[25] Z.L. Yu, N. Yang, L.C. Zhou, Z.Y. Ma, Y.B. Zhu, Y.Y. Lu, B. Qin, W.Y. Xing, T. Ma, S. C. Li, H.L. Gao, H.A. Wu, S.H. Yu, Bioinspired polymeric woods, Sci. Adv. 4 (8) (2018) eaat7223, https://doi.org/10.1126/sciadv.aat7223.
[26] B. Yuan, Q. Cheng, R. Zhao, X. Zhu, X. Yang, X. Yang, K. Zhang, Y. Song, X. Zhang, Comparison of osteointegration property between PEKK and PEEK: effects of surface structure and chemistry, Biomaterials 170 (2018) 116–126, https://doi.org/10.1016/j.biomaterials.2018.04.014.